Stability and precision studies of the LST-1 telescope

Author: Roger Petit Gozálvez, rpetitgoz@gmail.com
Facultat de Física, Universitat de Barcelona, Diagonal 645, 08028 Barcelona, Spain.

Advisors: Abelardo Moralejo, moralejo@ifae.es; Pol Bordas, pbordas@ub.edu

The Large-Sized Telescope prototype (LST-1) is crucial in the development of the Cherenkov Telescope Array (CTA). This study aims to improve the understanding of the stability and pointing precision of the LST-1. Using data from Crab Nebula, Markarian 421 (Mrk 421) and BL Lacertae (BL Lac), we analyze, for different timescales, whether the distributions of the reconstructed positions of the sources were centered on the expected positions. Additionally, we study the gamma-ray Point Spread Function (PSF) of the telescope to determine whether the spread of the reconstructed directions is consistent with those obtained from simulations. This analysis confirms the existence of a small pointing error which varies with time along the studied sample, in timescales larger than the run duration. Moreover, all results are consistent with a variable Gaussian mispointing for shorter timescales with a σ ranging from 0.63 ± 0.06 to 3.06 ± 0.06 arcmin, exhibiting a strong dependency on the telescope's position.
Keywords: Gamma-Ray Astronomy, Monte Carlo Simulations, Data Analysis
SDGs: 9.1 and 9.5

I. INTRODUCTION

The Large-Sized Telescope prototype (LST-1) is part of the next-generation ground-based observatory for gamma-ray astronomy: the Cherenkov Telescope Array [1]. CTA will provide access to the entire sky through a network of more than sixty telescopes distributed across two observatories, one in each hemisphere. The sensitivity and number of observable sources are expected to improve by an order of magnitude compared to previous projects such as HESS-II, MAGIC, and VERITAS. Substantial improvement of the angular and energy resolution is also expected [2]. Thus, specially the improvements on the sensitivity, brings us to the motivation behind this research: enhancing the stability and pointing accuracy of the telescope is crucial because inaccuracies in these aspects will be significantly less masked by statistical uncertainties.

The advances in gamma-ray astronomy with the CTA project are expected to deepen our understanding of the origin and role of relativistic cosmic particles, provide insights into cosmic ray acceleration mechanisms, and explore their connections to star formation rates and galaxy evolution. Furthermore, this research enables us to probe extreme environments near compact objects, such as neutron stars and black holes, while exploring frontiers in physics, including the nature and distribution of dark matter, quantum gravitational effects on photon propagation, and the potential existence of exotic particles such as axions. [3]

The observations will focus on the very-high energy (VHE) gamma-ray band, covering energies from 20 GeV to 300 TeV [2] with the LSTs being the telescopes capable of achieving the lowest energy threshold. The development in technology to study this energy range of the spectrum is particularly important for studying phenomena such as pulsars, supernova remnants and active galactic nuclei (AGN), which we analyze in this research.

In addition to Cherenkov telescopes, which offer a vast effective area due to the nature of their observational technique, there are also space-borne detectors, such as the Fermi-LAT, whose data were important for this research to provide the energy spectrum of the observed blazars in the GeV range. Space-borne detectors can observe regions of the electromagnetic spectrum that are inaccessible from the ground and have significantly contributed to the discovery of numerous high-energy gamma-ray sources. However, they also face critical limitations, including a much smaller effective area due to the size and weight constraints of satellite payloads [3]. Despite these differences, the complementary strengths of ground-based and space-borne detectors, along with contributions from other methods, together provide a comprehensive view of the upper range of the electromagnetic spectrum.

II. BACKGROUND

Imaging Atmospheric Cherenkov Telescopes (IACTs) rely on the detection of Cherenkov radiation produced by particle showers initiated in the upper atmosphere. When a gamma ray interacts with the atmosphere, it produces an electron-positron pair. Subsequently, these particles emit secondary gamma rays through the bremsstrahlung process, initiating the development of a particle shower. Due to the high energy of the gamma rays, the resulting charged particles can travel faster than the speed of light in the atmosphere, leading to the emission of Cherenkov radiation; which is processed to determine the direction and energy of the incoming gamma rays. [4]

However, one of the main challenges is that charged Cosmic Rays (CRs) also produce similar particle show-

ers. CRs, on the other hand, cannot be traced back to their sources due to deflection by galactic magnetic fields. Thus, they are not useful "astronomical messengers", and constitute instead the major part of the isotropic background noise recorded by IACTs.

As a result, a careful analysis of the recorded shower images is needed in order to identify the showers initiated by gamma rays among the much stronger cosmic-ray background. For this research, we used the DL2 data of LST-1, where key physical parameters, such as the energy and direction of the rays, have already been reconstructed. A crucial parameter, *gammaness*, is calculated using MC simulations of hadronic and gamma-ray showers, along with machine learning methods such as Random Forest (RF). This parameter represents a score (ranging from 0 to 1) which indicates how gamma-like a given shower is (with 0 meaning "most gamma-unlike", and 1 meaning "most gamma-like"), making it an essential parameter for filtering out the majority of the background.[3]

When observing VHE gamma rays from high-redshift sources, such as BL Lac and Mrk 421, the Extragalactic Background Light (EBL) plays a significant role, especially at higher energies. The EBL is the accumulated thermal emission from stars and galaxies and constitutes the bulk of the photon content of the universe in the optical and infrared wavelengths. Gamma rays interact with the EBL photons via pair production, leading to attenuation that limits the observable VHE gamma-ray flux from distant sources.

III. METHODOLOGY

We took as starting point a previous study [1] focused on observations of the Crab Nebula. In this research, it was determined indirectly, using Monte Carlo (MC) simulations, that the discrepancy in gamma-ray point-spread function (PSF) between the real data and the simulations was consistent with a variable Gaussian mispointing in both axes with $\sigma = 0.025°$ (1.5 arcminutes).

Therefore, we started working with DL2 data of the Crab Nebula due to the high quality of the available data (owing to its proximity and brightness in the gamma-ray band). Later on, we also studied important flares of BL Lac (4 and 9 of August, 2021) and Mrk 421 (18 May, 2022). These are extragalactic sources, which due to their large distance appear to us as point-like gamma-ray emitters. For the study of the LST-1 gamma PSF, this is an advantage with respect to the Crab Nebula, which is a slightly extended source.

The first thing that we had to be aware about, was that the mispointing can have different timescales and causes; depending on the nature of it, it was going to be easier or more difficult to determine it. Even for bright sources like the ones discussed here, the clear detection of the gamma-ray excess (clear enough to allow a study of the pointing and the PSF) requires the integration of at least a full data run (which typically lasts 20 minutes)

A. Odd-even study

The first approach was splitting the same data used for the paper mentioned before [1] into two independent sub-samples of equal statistics; which we did by separating the events according to their unique "event number" identifiers. We divided the sample into "odd event id" and "even event id". The two subsamples are statistically independent (no events in common), cover exactly the same observation periods, and share all other observation conditions, since the events are perfectly interleaved. This way, if a pointing deviation is observed and compatible across both subsamples, this would indicate that the effect is not primarily due to statistical fluctuations (though these are also present), but rather a systematic effect. The most plausible explanation in such a case would be mispointing.

We are interested in the reconstructed directions of gamma rays, which, even after the selection of gamma-like candidates, are mixed with a residual isotropic background of cosmic rays. In order to account for the effect of the background, we made use of the central symmetry of the camera and the fact that observations are performed in "wobble mode", in which the telescope is pointed 0.4 degrees away from the source of interest alternating between two different sky directions on opposite sides of the source[1]. Given this characteristic, we defined a region with a radius of approximately 0.3° around the source (ON). Analogously, we defined a symmetric region on the opposite side of the camera center (OFF), in which the background is expected to have the same characteristics as the background of the ON region (bg).

$$\Sigma_{\mathrm{bg}}\Delta x'_i \approx -\Sigma_{\mathrm{Off}}\Delta x'_j \qquad \text{(Symmetry about origin)}$$

We define and $\Delta x'_i$, $\Delta y'_i$ as the differences between the reconstructed position of each event and the center of ON and OFF (depending on the indexes i, j), for each axis. We use the indexes i,j to refer to each reconstructed event depending on whether it is located within the ON or OFF region, respectively. Therefore, we can determine the mean position of the gamma rays excess. Analogously, for each axis and with N as the number of events:

$$\frac{\Sigma_{\mathrm{On}}\Delta x'_i + \Sigma_{\mathrm{Off}}\Delta x'_j}{N_{\mathrm{On}} - N_{\mathrm{Off}}} \approx \frac{\Sigma_\gamma \Delta x'_i + \Sigma_{\mathrm{bg}}\Delta x'_i + \Sigma_{\mathrm{Off}}\Delta x'_j}{N_\gamma + N_{\mathrm{bg}} - N_{\mathrm{Off}}} \approx \frac{\Sigma_\gamma \Delta x'_i}{N_\gamma} \tag{1}$$

Where the right-hand term is the average deviation of the observed gamma-ray excess relative to the nominal source direction. In case of no mispointing we would obtain a value compatible with zero within statistical fluctuations

Then we applied different cuts in *gammaness* and intensity to study how the mean position of the gamma-ray excess (relative to the nominal source position), changes

over the runs for each sample and how correlated they were with each other.

To conclude, we performed a correction for the$\langle \Delta x_{odd} \rangle$ using the $\langle \Delta x_{even} \rangle$ values and vice versa for each run, in order to subtract the correlations presumably caused by mispointing; note that the prime symbol is omitted, as it is centered to the overall mean rather than the nominal position of the source. In addition, we tried to replicate the θ^2 distribution figure from the Crab Nebula observations paper [1] adding this corrected data to compare the results.

B. PSF study

On the other hand, we approached this problem differently by including the blazars Markarian 421 (Mrk 421) and BL Lacertae (BL Lac). In this case, we wanted to study the PSF of the telescope using blazars, as their coordinates are known with very high precision and, given their distance, they are really point-like for LST-1. Thus, in absence of mispointing, the distribution of reconstructed directions relative to the location of the source should be the PSF of the instrument.

For this method, we used data processed with the corresponding MC simulation developed by the CTA-LST team, which are modified depending on the orientation of the telescope in horizontal coordinates (Alt, Az). This is important because IACTs have a significant dependence on the pointing altitude due to variations in airmass, i.e., by the amount of atmosphere along the line of sight.

The MC events are generated with an energy spectrum $dF/dE \sim E^{-2}$. To ensure good data-MC agreement, energy-dependent weights are applied to the MC events to match the energy distribution of the observed source. Thus, this weights were calculated from the spectra obtained from the data analysis from Fermi and LST-1 [3] and considering the effects of the EBL on high-energy gamma rays over long distances based on Dominguez's model [5]. This was calculated for the spectrum of the flare in Mrk 421, as well as for the two flares observed in BL Lac.

To subtract the background, we first performed a Gaussian fit to all events located within a defined distance from the center. Then, we refined the fit by focusing only on the excess events near the peak to accurately determine its position. The background was then modeled using a first-degree polynomial fit applied to the events within the specified distance from the center. An example of this procedure is presented in FIG 7 in the supplementary material.

To conclude, we compared the real data with the weighted MC simulations, focusing on key statistical parameters. First of all, the difference between the mean position of the reconstructed excess and the nominal position of the source; the global mispointing. Moreover, we examined the standard deviation, σ, and the quadratic difference of variances, $\sqrt{|\sigma^2_{\text{data}} - \sigma^2_{\text{MC}}|}$, for each axis of the telescope camera. This metric is expected to be compatible with zero; if not, it indicates a potential variable mispointing, assuming Gaussian behavior.

IV. RESULTS

A. Odd-even study

We defined $\langle \Delta x \rangle$, $\langle \Delta y \rangle$ as the distance between the mean position of reconstructed events of each run and the overall mean along each axis of the camera; once the background is subtracted (using Eq. 1). A $gammaness > 0.94$ and $intensity > 750 p.e.$ cuts were applied to all the following plots in this section to conclude recreating the figure from the Crab Nebula observation paper where the corrected data is corrected also using this cuts.[1]

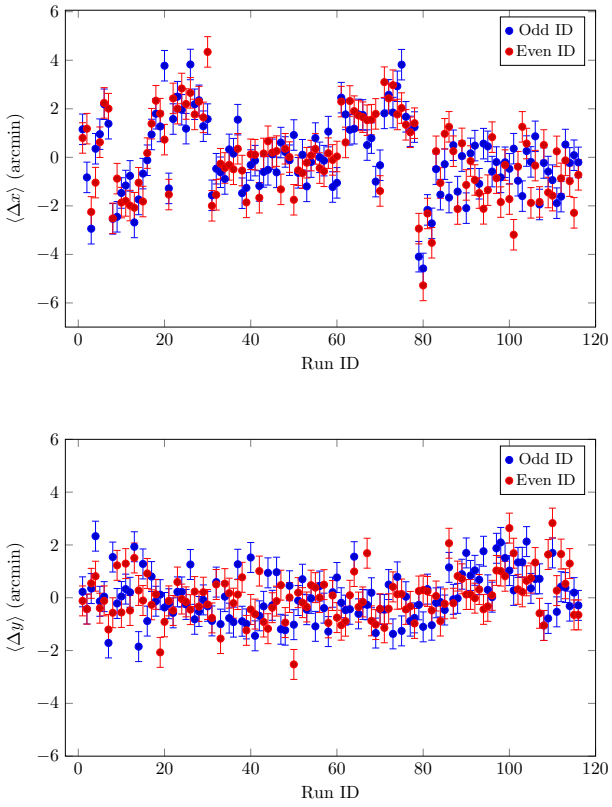

FIG. 1: Comparison of variations on $\langle \Delta x \rangle$ and $\langle \Delta y \rangle$, as a function of the run number, of two independent samples on Crab Nebula observations: odd and even event id's.

The top graph of FIG. 1, illustrates $\langle \Delta x \rangle$ along 117 runs that were taken within approximately 1,5 years. We can observe variations on $\langle \Delta x \rangle$ across the runs are similar for the two independent samples on a scale of tens of runs. We would not expect any correlation if the deviations of $\langle \Delta x \rangle$ were purely statistical, as the samples don't share

events. During this period, adjustments were made to the pointing calibration software, which may have contributed to the observed variations. Additionally, it is important to note that the data from run 85 were collected shortly after the end of the volcanic eruption in La Palma, near the telescope. It is debatable whether the dispersion of the data increased as a result of this event.

Although the bottom graph in FIG.1 shows a similar dispersion compared to the X-axis (similar error bars), it is clear that no reproducible pattern is observed across both samples. We attribute this behavior to the fact that the bending of the telescope, caused by the weight of the camera and its supporting structure, induces variable deformation along the zenith axis. This deformation is corrected by the bending model integrated into the telescope's drive software, which adjusts the pointing calculations to ensure accuracy. Consequently, differences in this axis are expected to be more pronounced during recalibration of the telescope's drive, as opposed to the azimuthal axis, where gravitational asymmetry is not a factor.

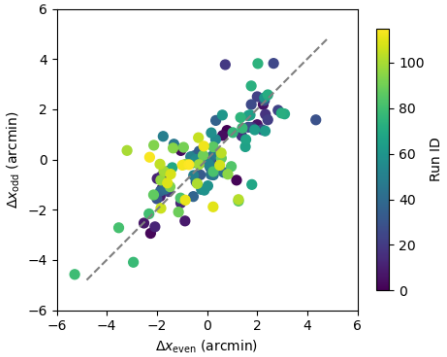

FIG. 2: Correlation between $\langle \Delta x_{odd} \rangle$ and $\langle \Delta x_{even} \rangle$ for the Crab Nebula observations, coinciding with the zenith axis of the telescope.

FIG. 2 enables a more detailed analysis of the correlation between the samples, where a significant relationship is observed. Furthermore, the calculated Pearson correlation coefficient r ≈ 0.74 confirms a notable degree of correlation between the two samples. This result indicates the presence of mispointing at this timescale, however, there is considerable dispersion between the data and the adjustment of perfect correlation ($\sigma \approx 1,15$ arcmin).

FIG. 3 aims to replicate the figure presented in the referenced paper [1] , where θ^2 represents the squared angular distance between the reconstructed event directions and the source, corrected for global mispointing. This replication is done to compare the results after applying correction. The correction is calculated by subtracting $\langle \Delta x_{odd} \rangle$ from $\langle \Delta x_{even} \rangle$, and vice versa, thereby eliminating the correlation caused by mispointing. A small, but significant improvement compared to the error bars, can

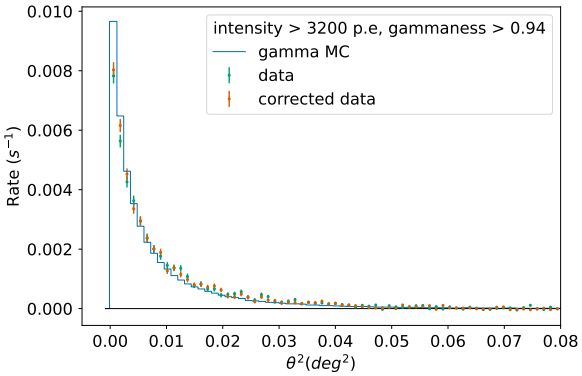

FIG. 3: θ^2 distribution for the Crab Nebula excess events.

be observed in the agreement between the MC simulation (which considers the source as a Gaussian distribution) and the reconstructed data.

B. PSF study

Source		BL Lac		Mrk 421
Flare		4 August, 2021	9 August, 2021	18 May, 2022
Peak$_{excess}$ (arcmin)	x	0.2 ± 0.2	-0.4 ± 0.3	0.0 ± 0.2
	y	0.6 ± 0.4	0.3 ± 0.3	5.4 ± 0.6
σ_{data} (arcmin)	x	3.9 ± 0.2	4.1 ± 0.3	5.0 ± 0.3
	y	5.1 ± 0.3	4.8 ± 0.3	5.0 ± 0.3
$\sqrt{\lvert\sigma^2_{data} - \sigma^2_{MC}\rvert}$	x	0.9 ± 0.2	0.9 ± 0.3	3.6 ± 0.3
	y	3.1 ± 0.3	2.6 ± 0.3	0.6 ± 0.3
σ_{corr} (arcmin)	x	0.66 ± 0.06	0.90 ± 0.06	3.06 ± 0.06
	y	2.70 ± 0.06	2.22 ± 0.06	0.63 ± 0.06
Zenith range		$14° - 49°$	$14° - 32°$	$17° - 29°$
Azimuth range		$332° - 58°$	$354° - 55°$	$296 - 307°$

TABLE I: Results of the PSF study for Mark 421 and BL Lac flares, along with a comparison to the MC simulations (in arcminutes). The standard deviation of the smearing applied to achieve perfect agreement between the real data and the MC, as well as the range of the telescope's observations.

The first obtained result was the position of the peak of the Gaussian fit for the excess, which corresponds to the reconstructed position of the source respect to the nominal position of it. For all cases, it is considerably smaller than for Crab Nebula: 1.12 ± 0.06 and 0.74 ± 0.05 arcmin. This could be due to that the position of Crab Nebula is not determined on the gamma-ray band, and given it's extension on the sky we may be introducing a general mispointing.

Another observation from the results presented in Table 1 is the similarity between the two flares of BL Lac.

This outcome aligns with expectations, as both flares originate from the same source, correspond to the same region of the sky, and have comparable spectra. However, these findings differ from those obtained in studies of the Crab Nebula, where a greater mispointing along the X-axis was anticipated. Thus, it does not support our previous hypothesis, which attributed a lower pointing precision along this axis to telescope bending and potential imperfections in its correction mechanisms.

It is important to note that these results are consistent with the interpretation that the variations observed on $\langle \Delta x \rangle$ in FIG. 1 are attributable to mispointing, given that the timescale of the fluctuations in that case is longer than the timescale of these observations; with similar fluctuations on shorter timescales for both axes.

For Mrk 421, we observe a significantly greater mispointing along the X-axis, in contrast to the results obtained for BL Lac. In summary, this suggests that the dependency of mispointing on the axes is primarily influenced by the direction in which the telescope is pointed, as expected. Although the zenith and azimuth ranges are similar, the observation times differ in each case. For the Crab Nebula, the maximum observation time occurs at a zenith angle of 6°.

V. CONCLUSIONS

In this study, we have analyzed the stability and precision of the LST-1 telescope using multiple methods, focusing on both galactic and extragalactic gamma-ray sources. Our findings confirm for the Crab Nebula observations, that a portion of the observed mismatch in the PSF between real data and MC simulations arises from mispointing along the X-axis. This axis of the camera coincides with the vertical axis where the telescope bends, complicating the pointing calibration. This problem is known and corrected with the "bending model", however, as this mispointing is observed at high timescales (Crab Nebula observations within approximately 1,5 years), we attribute it to adjustments on the parameters to the telescope's "bending model" software during the commissioning of the telescope.

All the results obtained from section B are compatible with a with a Gaussian mispointing smearing. However, the global mispointing is relatively low. Given the fact that the observations of this sources were short, it indicates a mispointing at short timescales, which is also compatible with the results obtained with Crab Nebula. The dependency on both axes seems to be just related with the position of the telescope during the observations. A detailed analysis of the mispointing variations across different zenith angles could provide further insight into this issue.

It could be possible that a part of the discrepancy observed between the data and MC simulations in the PSF study could be attributed to an oversimplification in the MC simulations. For instance, the noise generated by nearby stars contributes to the complexity of accurately reconstructing the directions of particle showers, which is not well reproduced on the simulations. However, the effect is expected to be negligible .

To delve on this study, the implementation of the Star Tracking System [6], which observes stars in the field of view to improve pointing accuracy, is expected to provide valuable insights.This program could help determine whether the discrepancies are entirely due to mispointing or if other short-timescale phenomena contribute as well. Moreover, it will play a key role in correcting these issues and enhancing the telescope's pointing precision.

Acknowledgments

I would like to thank the High Energy Physics Institute (IFAE) for this opportunity, and especially my advisor, Dr. Abelardo Moralejo, for his unconditional guidance and support, which I truly appreciate. His enthusiasm and professionalism are qualities I deeply admire. I would also like to thank Dr. Pol Bordas for his help as my advisor at the University of Barcelona, as well as my family.

[1] C.-L. Project, S. Abe, A. Aguasca-Cabot, I. Agudo, et al., *Observations of the crab nebula and pulsar with the large-sized telescope prototype of the cherenkov telescope array* (2023), version: 2, 2306.12960 [astro-ph], URL `http://arxiv.org/abs/2306.12960`.

[2] C. T. A. Consortium, B. S. Acharya, I. Agudo, et al., *Science with the Cherenkov Telescope Array* (2018), version: 2, 1709.07997 [astro-ph], URL `http://arxiv.org/abs/1709.07997`.

[3] C. S. Priyadarshi, *Observation of active galactic nuclei in the gamma-ray band using the first telescope of the CTA north*, 2024-07-09 (Tesis Doctorals en Xarxa), URL `http://hdl.handle.net/10803/691736`.

[4] M. d. Naurois and D. Mazin, **16**, 610 (2015), ISSN 1878-1535, 1511.00463 [astro-ph], URL `http://arxiv.org/abs/1511.00463`.

[5] A. Domínguez, J. R. Primack, et al., **410**, 2556 (2011), ISSN 0035-8711, URL `https://doi.org/10.1111/j.1365-2966.2010.17631.x`.

[6] K. Abe, S. Abe, et al., **679**, A90 (2023), ISSN 0004-6361, 1432-0746, publisher: EDP Sciences, URL `https://www.aanda.org/articles/aa/abs/2023/11/aa47128-23/aa47128-23.html`.

Estudi de l'estabilitat i precisió del telescopi LST-1

Author: Roger Petit Gozálvez, rpetitgoz@gmail.com
Facultat de Física, Universitat de Barcelona, Diagonal 645, 08028 Barcelona, Spain.

Advisors: Abelardo Moralejo, moralejo@ifae.es; Pol Bordas, pbordas@ub.edu

Resum: El prototip *Large-Sized Telescope* (*LST-1*) és essencial per al desenvolupament del *Cherenkov Telescope Array* (*CTA*). Aquest estudi té com a objectiu entendre millor la precisió i l'estabilitat del *LST-1* per aplicar els resultats als futurs telescopis del *CTA*. S'han analitzat dades de la Nebulosa del Cranc, *Markarian 421* (*Mrk 421*) i *BL Lacertae* (*BL Lac*) en diferents escales temporals per determinar si les posicions reconstruïdes de les fonts coincideixen amb les posicions esperades. A més, s'ha estudiat la *Point Spread Function* (*PSF*) per verificar si l'amplada de les direccions reconstruïdes és coherent amb les simulacions. L'anàlisi confirma un desajustament en l'eix vertical de la càmera (eix X) en escales de temps llargues. També s'observa un desajustament gaussià variable en escales curtes, amb σ entre 0.63 ± 0.06 i 3.06 ± 0.06 minuts d'arc, depenent de la posició del telescopi.
Paraules clau: Astronomia de rajos gamma, Anàlisis de Dades.
ODSs: Aquest TFG esta relacionat amb els SDGs 9.1 i 9.5

SUPPLEMENTARY MATERIAL (OPTIONAL)

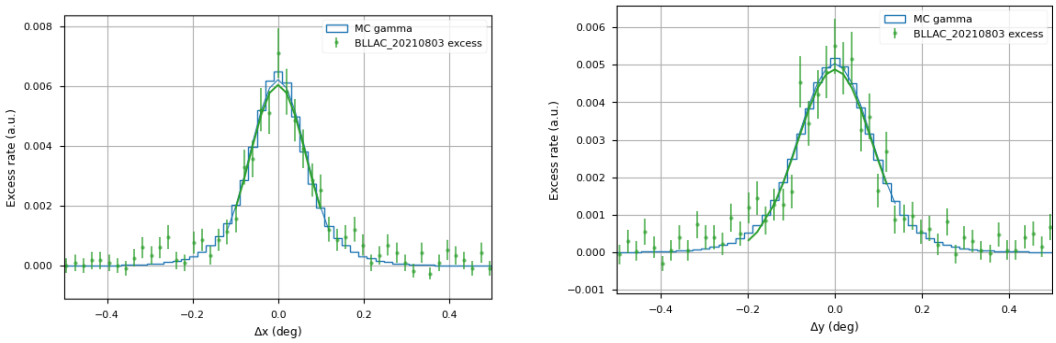

FIG. 4: PSF study for the X and Y axes of the LST-1 camera. Comparison of real data with MC simulations with the applied smearing correction. BL Lac during the flare observed on 04/08/2021.

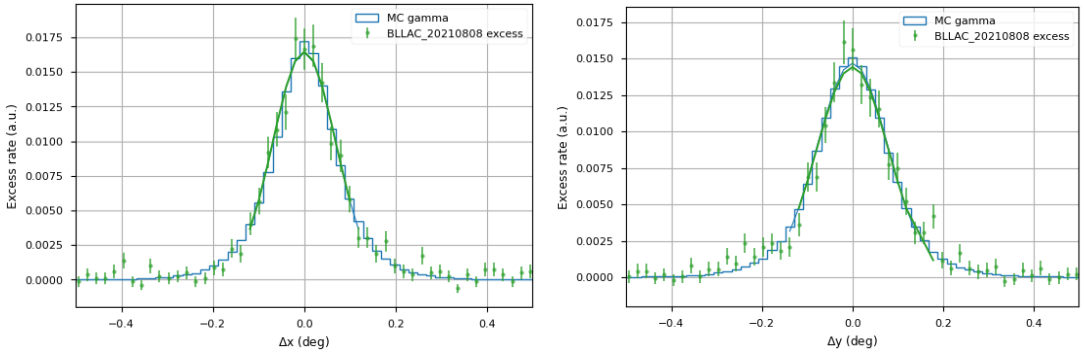

FIG. 5: PSF study for the X and Y axes of the LST-1 camera. Comparison of real data with MC simulations with the applied smearing correction. BL Lac during the flare observed on 09/08/2021.

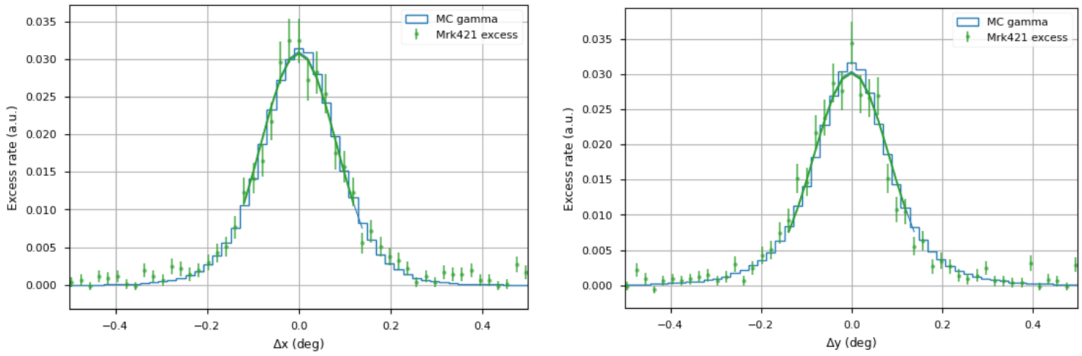

FIG. 6: PSF study for the X and Y axes of the LST-1 camera. Comparison of real data with MC simulations with the applied smearing correction. Mrk 421 during the flare observed on 18/03/2021.

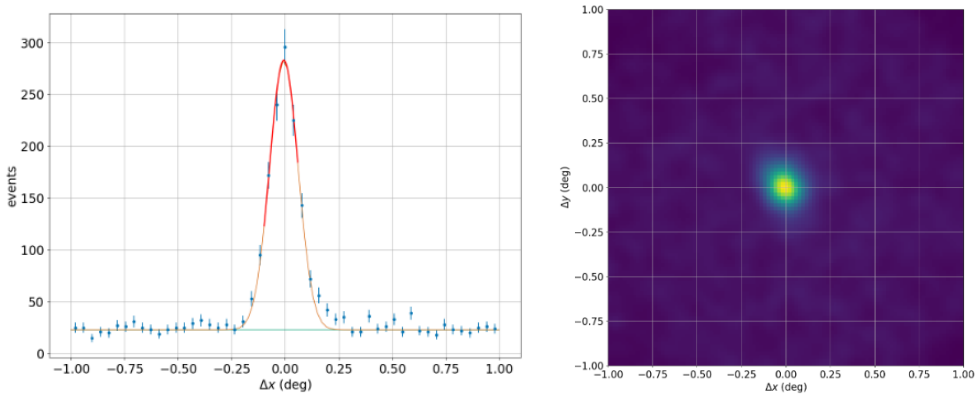

FIG. 7: Example of the BL Lac flare observed on 09/08/2021, showing the Gaussian fit to the peak excess and the linear fit to the background. On the right, a sky map with a gaussian filter of $\sigma = 0.04°$ showing the number of events with colors